ACS APPLIED MATERIALS & INTERFACES
Research Article
www.acsami.org

Multiscale Assembly of Grape-Like Ferroferric Oxide and Carbon Nanotubes: A Smart Absorber Prototype Varying Temperature to Tune Intensities

Ming-Ming Lu,[†] Mao-Sheng Cao,[*,†] Yi-Hua Chen,[†] Wen-Qiang Cao,[‡] Jia Liu,[†] Hong-Long Shi,[‡] De-Qing Zhang,[†] Wen-Zhong Wang,[‡] and Jie Yuan[*,‡]

[†]School of Material Science and Engineering, Beijing Institute of Technology, Beijing, 100081, China
[‡]School of Science, Minzu University of China, Beijing, 100081, China

Supporting Information

ABSTRACT: Ideal electromagnetic attenuation material should not only shield the electromagnetic interference but also need strong absorption. Lightweight microwave absorber with thermal stability and high efficiency is a highly sought-after goal of researchers. Tuning microwave absorption to meet the harsh requirements of thermal environments has been a great challenge. Here, grape-like Fe_3O_4-multiwalled carbon nanotubes (MWCNTs) are synthesized, which have unique multiscale-assembled morphology, relatively uniform size, good crystallinity, high magnetization, and favorable superparamagnetism. The Fe_3O_4-MWCNTs is proven to be a smart microwave-absorber prototype with tunable high intensities in double belts in the temperature range of 323−473 K and X band. Maximum absorption in two absorbing belts can be simultaneously tuned from ∼−10 to ∼−15 dB and from ∼−16 to ∼−25 dB by varying temperature, respectively. The belt for reflection loss ≤−20 dB can almost cover the X band at 323 K. The tunable microwave absorption is attributed to effective impedance matching, benefiting from abundant interfacial polarizations and increased magnetic loss resulting from the grape-like Fe_3O_4 nanocrystals. Temperature adjusts the impedance matching by changing both the dielectric and magnetic loss. The special assembly of MWCNTs and magnetic loss nanocrystals provides an effective pathway to realize excellent absorbers at elevated temperature.

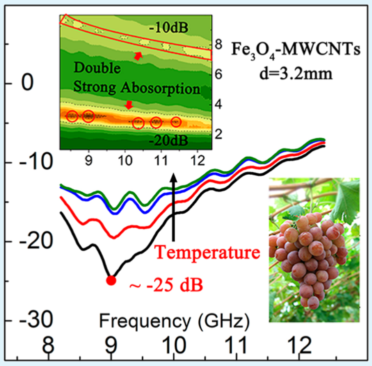

KEYWORDS: *smart absorber, carbon nanotube, magnetic ferroferric oxide, multiscale assembly, temperature dependence*

INTRODUCTION

With the rapid increase of electric information technology, such as the high speed processors, information counterwork, satellite communication, and broadband radar, the negative influence from electromagnetic radiation on the environment and human health has become increasingly severe. Electronic devices can generate considerable heat emission and release undesirable electromagnetic radiation, which would compromise the function and lifetime of the nearby electric components. An ideal electromagnetic attenuation material could not only shield the electromagnetic interference (EMI) but also exhibit strong absorption to keep the surrounding environment clear. Additionally, the heat emission would also influence the performance of attenuation materials. Therefore, tuning microwave absorption (MA) to meet the harsh requirements of thermal environments has been a great challenge. Thermally stable, highly efficient, and lightweight MA materials are highly demanded to attenuate and even eliminate adverse electromagnetic waves effectively in a wide range of processes including national defense security, electronic safety, healthcare, and so on.[1−5]

Some kinds of conventional MA candidates, such as ferroelectric, ferrites, and carbides, are widely investigated.[6−8] Although good MA performance appears in some cases, the drawbacks, including high density, large thickness, and high loading content, have severely limited their practical applications. In recent years, carbon materials, such as ordered mesoporous carbon,[9] carbon nanotubes,[10−18] carbon nanocoils,[4] reduced graphene oxides and graphene,[19−28] etc., have exhibited potential application in MA. Multiwalled carbon nanotubes (MWCNTs) and their heterostructures, as lightweight absorbers, have been extensively researched due to the high specific surface areas and carrier mobility.[29−35] Unfortunately, pure MWCNTs or the ones decorated with dielectric loss materials suffer from improper electrical conductivity or poor impedance matching due to single dielectric loss. It has been realized that the combination of dielectric and magnetic loss materials could be an effective solution to improve MA capacity.[36−49] Fe_3O_4 nanoparticles are important magnetic functional nanomaterials with extensive applications. They have been proven to exhibit potential MA properties whenever they are the only component or one component in heterostructures.[50−52] However, the applications of MA materials should pay great attention to harsh thermal environment factors. Only

Received: June 23, 2015
Accepted: August 18, 2015
Published: August 18, 2015

DOI: 10.1021/acsami.5b05595
ACS Appl. Mater. Interfaces 2015, 7, 19408−19415

Scheme 1. (A−D) The Synthesized Process of Grape-Like Fe_3O_4-MWCNTs; (E) Photograph of SiO_2-Matrix Composite Loading with Fe_3O_4-MWCNTs for Dielectric Test; (F) SEM Image of the Multiscale-Assembled Grape-Like Fe_3O_4-MWCNTs

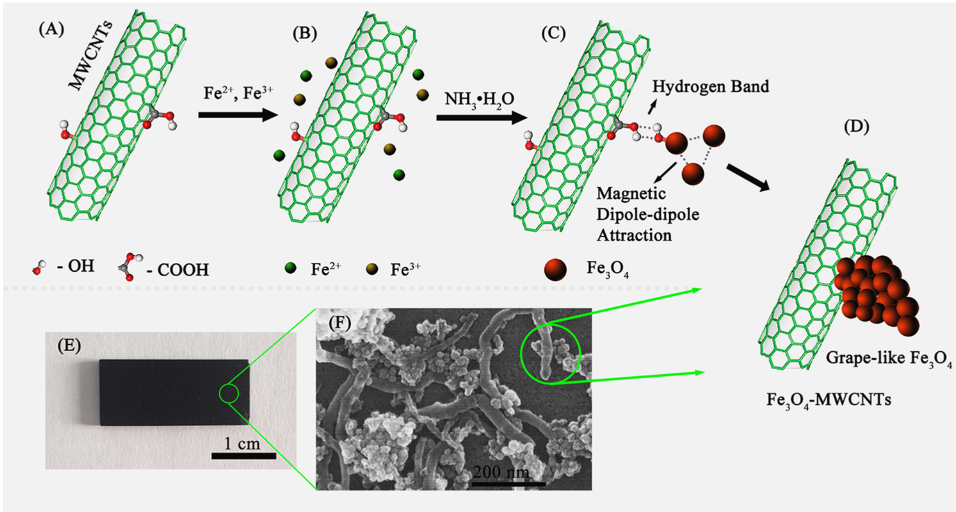

few works have focused on the evolution law of MA performance with changing temperature.[6,53] More important, the study on the electromagnetic impedance matching of magnetic material/dielectric material at elevated temperature still remains unexplored up to date. In addition, although there have been works on the MA capacity of MWCNT decorated with Fe_3O_4 particles, all the microstructures of the hybrids are similar and single.[38,54,55] Novel microstructures of the hybrids of MWCNT and Fe_3O_4 deserve to be further studied. In our previous work, we have fabricated a hybrid with new microstructure consisting of MWCNT and Fe_3O_4 crystals. This work is the further investigation of our previous work.[56]

Here, we fabricated multiscale-assembled grape-like Fe_3O_4-MWCNTs by coprecipitation. We demonstrated dielectric and MA properties of the nanostructure in the temperature range of 323−473 K and X band. Results show that the nanostructure possesses double-belt absorption; the maximum absorptions are −24.8 and −14.3 dB in the belts, separately. The belt for reflection loss (RL) ≤ −20 dB can almost cover the X band at 323 K. More significantly, the double belts can be simultaneously tuned by varying temperature, which confirms that the grape-like Fe_3O_4-MWCNTs is a promising prototype for lightweight and smart absorber at elevated temperature.

■ RESULTS AND DISCUSSION

The synthesized process of Fe_3O_4-MWCNTs is shown in Scheme 1A−D. The supernatant containing well dispersed MWCNTs can be obtained by treating the neutral aqueous solution of the acid-treated MWCNTs with ultrasonic cell disruptor. Without drying treatment, the supernatant was concentrated and directly added with $NH_4Fe(SO_4)_2{\cdot}12H_2O$ and $(NH_4)_2Fe(SO_4)_2{\cdot}6H_2O$. This process could keep the dispersity of MWCNTs in the solution. As shown in Scheme 1C,D, Fe_3O_4 nanocrystals were synthesized by the coprecipitation of Fe^{2+} and Fe^{3+} under the presence of $NH_3{\cdot}H_2O$. The Fe_3O_4 nanocrystals were bounded on the MWCNTs probably through the hydrogen band. The combination among Fe_3O_4 nanocrystals is likely aroused by the magnetic dipole−dipole attraction.[57] Products with different reaction times (5, 15, and 30 min) were collected to study the synthesized process, Sample I, Sample II, and Sample III, respectively. Figure S1 shows the morphology of three samples. First, one or several Fe_3O_4 nanocrystals are immobilized on the MWCNTs; then, the nanocrystals are assembled into Fe_3O_4 clusters, which finally become bigger to be grape-like clusters. Scheme 1F reveals a macroscopic assembly of the network interconnected by individual MWCNTs or Fe_3O_4 clusters. Scheme 1D−F exhibits the multiscale assembly of grape-like Fe_3O_4 and MWCNTs.

The crystal structure of the end-product Sample III was identified by the X-ray diffraction (XRD) patterns in Figure 1A.

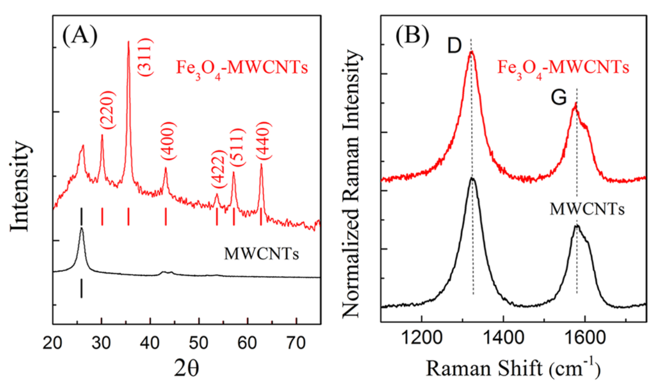

Figure 1. XRD (A) and Raman spectrum (B) of grape-like Fe_3O_4-MWCNTs and pure MWCNTs.

All the diffraction peaks marked with red bars can be indexed to the cubic spinel structure of Fe_3O_4. No other diffraction peaks of impurities could be found.[50] The characteristic peak centered at ∼26.5° indicates that MWCNTs were well preserved during the synthesis process of the heterostructures, which could also be proven by the almost unchanged intensity ratio of D and G band in the Raman spectrum of Fe_3O_4-MWCNTs and pure MWCNTs in Figure 1B.

The micromorphology of Sample III is shown in Figures 2 and 3. As shown in Figure 2A,B, several or dozens of Fe_3O_4 nanocrystals aggregate and are bounded on the MWCNTs, which look like grape clusters hung on the grapevine as shown in Figure 2C. The scanning electron microscopy (SEM) images in Figure 2D show that grape-like Fe_3O_4 nanocrystal clusters

DOI: 10.1021/acsami.5b05595
ACS Appl. Mater. Interfaces 2015, 7, 19408−19415

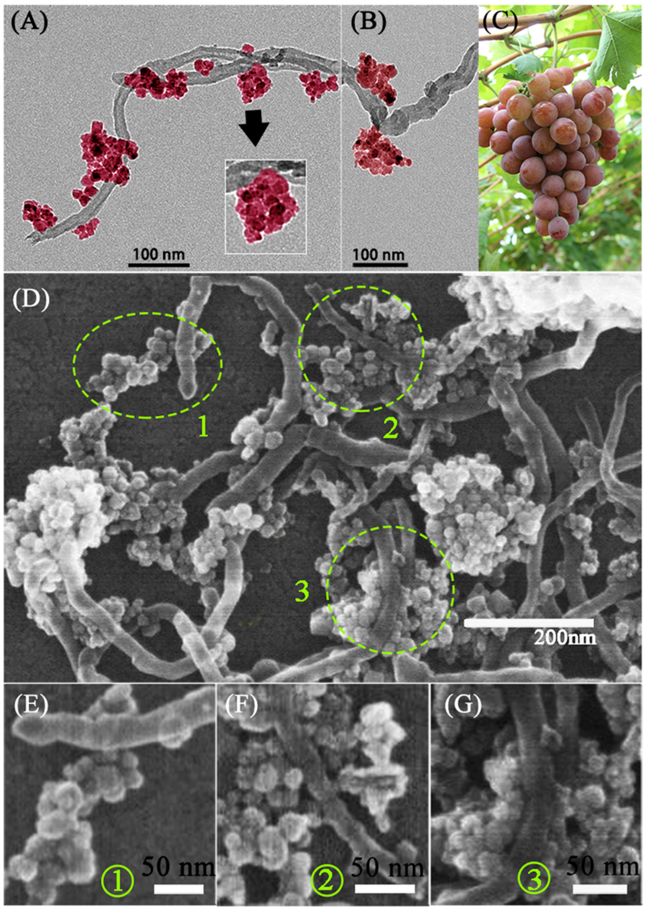

Figure 2. (A, B) Colored TEM images of multiscale-assembled grape-like Fe_3O_4-MWCNTs; (C) photograph of a bunch of grapes; (D) SEM image of the Fe_3O_4-MWCNTs with various morphologies; (E–G) three kinds of morphologies magnified from the green circles 1, 2, and 3 in (D), respectively.

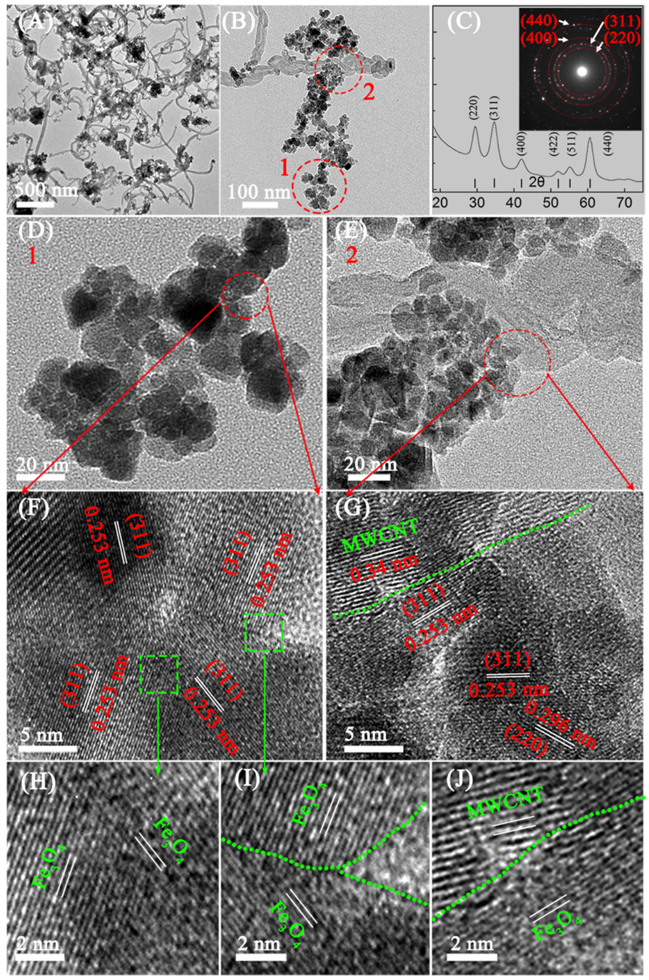

Figure 3. (A, B) TEM images of multiscale-assembled grape-like Fe_3O_4-MWCNTs with different magnifications; (C) diffraction profile generated by the SAED pattern of the Fe_3O_4-MWCNTs, the inset was recorded from the region of (B); (D, E) magnified TEM images of the regions marked with red circles 1 and 2 in (B), respectively; (F, G) high-resolution TEM images of the regions marked with red circles at (D) and (E); (H–J) the combination situation among Fe_3O_4 nanocrystals and MWCNTs.

are randomly decorated on the MWCNTs. Figure 2E shows that one grape-like Fe_3O_4 nanocrystal cluster is hung on the MWCNT. Figure 2F,G shows the other situations of the junctions between MWCNTs and the clusters. The transmission electron microscopy (TEM) images in Figure 3A,B further infer that grape-like Fe_3O_4 nanocrystals are decorated on the MWCNT. Figure 3C is the diffraction profile generated by the inserted SAED pattern, which indicates the cubic spinel structure of Fe_3O_4, keeping consistent with the XRD results. As shown in Figure 3D,E, the Fe_3O_4 nanocrystals with relatively uniform size are spherical and mostly around 6–16 nm in diameter. The particle size distribution of Fe_3O_4 nanocrystals is relatively concentrated (Figure S2). Adjacent Fe_3O_4 nanocrystals grow together tightly; the Fe_3O_4 nanocrystals are bounded on the surface of the MWCNT as shown in Figure 3F,G. The interfaces marked with a green dashed line in Figure 3H–J further indicate that the lattice mismatch generates abundant interfaces among dozens of Fe_3O_4 nanocrystals and MWCNTs. These interfaces generate polarizations and capacitor-like structures, which have significant influences on the dielectric and electrical properties of grape-like Fe_3O_4-MWCNTs.

The magnetic properties of Sample I, Sample II, and Sample III were determined by a vibrating sample magnetometer. It can be seen in Figure 4A that grape-like Fe_3O_4-MWCNTs dispersed in deionized water can be rapidly separated within 1 min by an external magnetic field. This phenomenon can be further supported by the hysteresis loops of Sample III with a saturation magnetization of 50.3 emu/g in Figure 4B. The saturation magnetization gradually increased with the increase of Fe_3O_4 amount on the MWCNTs. The Fe_3O_4-MWCNTs show no remanence or coercivity, indicating the Fe_3O_4 nanocrystal cluster possesses superparamagnetism. It is probably due to the cluster consisting of small nanocrystals with 6–16 nm diameter, thus retaining their superparamagnetism, while Fe_3O_4 crystals with microsize commonly exhibit ferromagnetic behavior.[50,58] The saturation magnetization aroused by Fe_3O_4 sufficiently improves the complex permeability of the Fe_3O_4-MWCNTs.

The real permittivity (ε'), imaginary permittivity (ε''), real permeability (μ'), and imaginary permeability (μ'') of the samples loading with grape-like Fe_3O_4-MWCNTs (Sample III) were investigated in the frequency range of 8.2–12.4 GHz and temperature range of 323–473 K. As shown in Figure 5A,C,E, both the ε' and ε'' of the Fe_3O_4-MWCNTs samples present an increasing trend with the increase of grape-like Fe_3O_4-MWCNTs loading, changing from 3.0 to 8.5 and 0.17 to 8.5,

DOI: 10.1021/acsami.5b05595
ACS Appl. Mater. Interfaces 2015, 7, 19408–19415

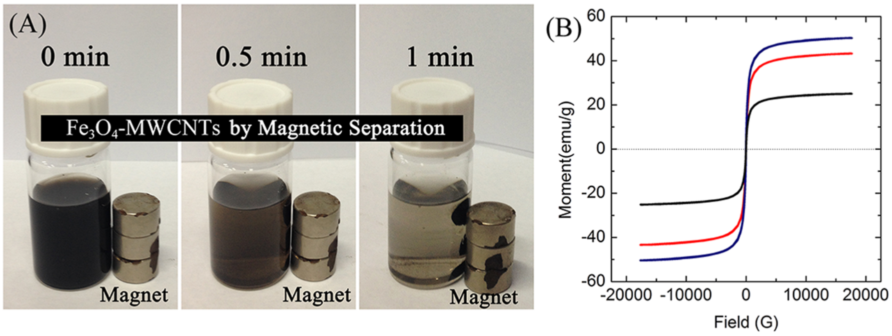

Figure 4. (A) The experiment for magnetism and (B) VSM results of the Fe_3O_4-MWCNTs. Black, red, and blue lines are for Sample I, Sample II, and Sample III, respectively.

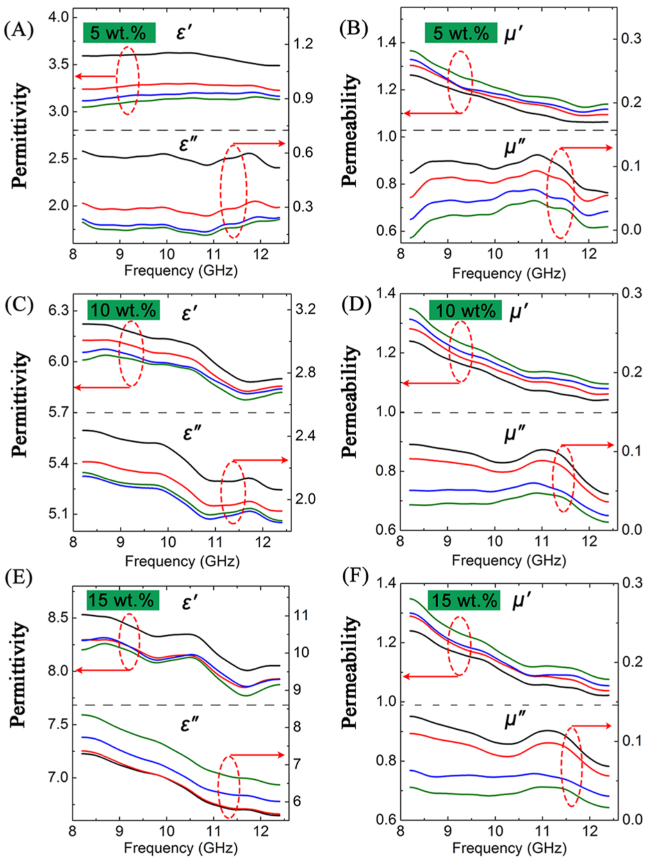

Figure 5. Plots of the complex permittivity and complex permeability at 323 K (black line), 373 K (red line), 423 K (blue line), and 473 K (green line) of the samples with (A, B) 5 wt %, (C, D) 10 wt %, and (E, F) 15 wt % grape-like Fe_3O_4-MWCNTs loading versus frequency.

respectively. Both the ε' and ε'' decrease with the increase of frequency. The relaxation peaks for ε'' are observed at ~9.9 and ~11.7 GHz. The ε'' of the samples with 5 and 10 wt % loading decreases with increasing temperature, while the ε'' for 15 wt % loading monotonically increases with increasing temperature in the range of 323 to 473 K. The ε'' demonstrates different temperature dependences with the changing Fe_3O_4-MWCNTs loading, which could also be seen in Figure S3, referring to the increasing degree of dipole orientation and the decreasing internal friction aroused by the rotation of the dipoles with elevated temperature.[19,59] Similarly, the dielectric loss tangent ($\tan \delta_e$) of the samples with 5 and 10 wt % loading decreases and increases for 15 wt % loading at elevated temperature (Figure S4).

In Figure 5B,D,F, both the μ' and μ'' indicate a decreasing trend with the increase of frequency. All the μ'' of the samples with different loading concentrations decreases with the increase of temperature. The relaxation peak for μ'' is observed at ~11.0 GHz. The μ' and μ'' range from 1.1 to 1.4 and 0 to 0.13, respectively. As shown in Figure S4, the maximum values of the magnetic loss tangent ($\tan \delta_m$) reach to 0.11. All the $\tan \delta_m$ of the samples with 5, 10, and 15 wt % loading show a decreasing trend with increasing temperature. This phenomenon is attributed to the weakening effects of temperature to magnetism.

MA properties were investigated by the reflection loss (RL), which is calculated using the relative complex permittivity and permeability according to the transmit line theory. RL is defined as in the following equations:

$$RL(dB) = 20\log_{10}|Z_{in} - Z_0/Z_{in} + Z_0| \quad (1)$$

$$Z_{in} = \sqrt{\mu_r/\varepsilon_r}\tan h[j(2\pi/c)\sqrt{\mu_r/\varepsilon_r}fd] \quad (2)$$

where ε_r and μ_r are relative complex permittivity and permeability of the absorber, respectively; Z_{in} is the normalized input impedance of the absorber; Z_0 represents the impedance of free space; f is microwave frequency; c is the light velocity; d is the coating thickness. As shown in Figure 6A,B, the RL of the sample with 10 wt % grape-like Fe_3O_4-MWCNTs loading is much better than that of the sample with equal MWCNTs loading concentration and same sample thickness d of 3.2 mm. The minimum RL of the Fe_3O_4-MWCNTs sample is about 3.3 times larger than that of the MWCNTs sample. When changing the d, the maximum MA of the MWCNTs sample could be achieved at the d of 2.1 mm. It can reach ~−10 dB, which is still quite weaker than that of the Fe_3O_4-MWCNTs sample (Figure S5). The bandwidth of the sample with10 wt % grape-like Fe_3O_4-MWCNTs loading reaches about 3.7 GHz for RL ≤−10 dB in the whole test temperature range of 323−473 K, which almost covers the full X band.

Perfect MA materials need the synergy of dielectric loss and magnetic loss. As a result, the input impedance of the MA materials is closer to the impedance of free space, and more energy of the incident EM waves can be attenuated inside the absorbers, leading to a high efficiency EM absorption. Therefore, the introduction of magnetic loss is very important for the enhancement of MA performance. In this work, the enhanced MA properties of Fe_3O_4-MWCNTs samples are attributed to the synergistic effect between dielectric MWCNTs

DOI: 10.1021/acsami.5b05595
ACS Appl. Mater. Interfaces 2015, 7, 19408−19415

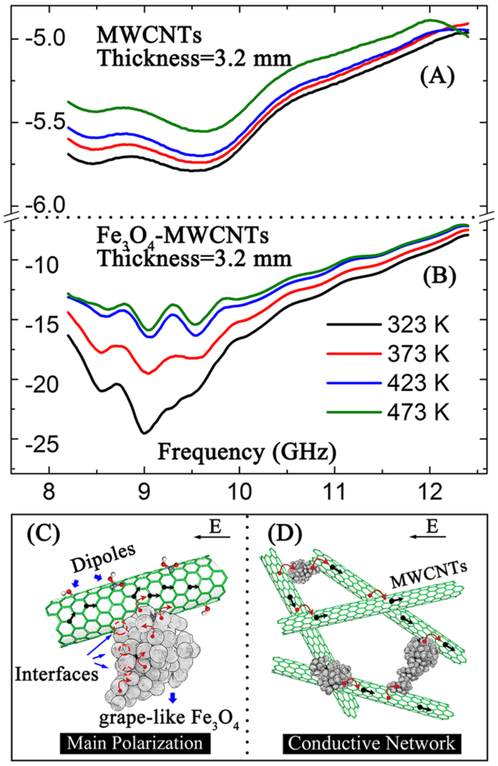

Figure 6. Microwave absorption properties of the samples (A) loaded with 10 wt % MWCNTs versus that of the samples (B) loaded with 10 wt % grape-like Fe_3O_4-MWCNTs; (C, D) The illustration for main polarizations and conductivity pathways. Red arrows represent hopping electrons; black arrows represent migrating electrons.

and magentic Fe_3O_4 nanocrystals. According to the Debye theory, the ε'' represents the dielectric loss, which consists of both polarization loss and conductivity loss. The polarizations include the interfacial polarizations existing in the abundant interfaces among grape-like Fe_3O_4 nanocrystals and MWCNTs, as well as the dipole polarizations caused by surface functional groups, defects on/in treated MWCNTs as shown in Figure 6C.[42] Meanwhile, due to 1D structure and high conductivity σ of MWCNTs, Fe_3O_4-MWCNTs can build a conductive network in the sample for electrons hopping and migrating as shown in Figure 6D. The formation of the network may also benefit from increased conductive pathways aroused by Fe_3O_4 clusters. Figure S6 shows the ε'' contributed by the σ (ε''_c) of the composites with 5, 10, and 15 wt % grape-like Fe_3O_4-MWCNTs loading. With the increase of loading concentration, the σ increases, and the ε''_c also increases considerably. However, it can be seen that ε''_c is less than 0.05, which is much smaller than all the ε'' for the samples with all three loading concentrations. Therefore, the polarization loss is a main contribution to the dielectric loss of the Fe_3O_4-MWCNTs samples.

The magnetic loss also contributes to the MA performance. The magnetic loss of the samples probably originates from exchange resonance,[39,42] which could be enhanced becuase the radii of Fe_3O_4 nanocystals fall in the range of the exchange length ~10 nm.[7,60,61] Natural resonance generally appears at low frequency below 8.2 GHz, and the eddy current loss in the Fe_3O_4-MWCNTs can also be ignored according to the unsteady value of $\mu''(\mu')^{-2}f^{-1}$ for the samples with different loading concentrations under various temperatures in Figure 7.[39,42]

The Fe_3O_4 amount on the MWCNTs, loading concentration, sample thickness, and temperature have significant effects on the MA performance of the samples loading with grape-like Fe_3O_4-MWCNTs. The sample with 10 wt % loading has better MA than the samples with 5 and 15 wt % loading (Figure S7). In Figure 8A–D, the sample with 10 wt % loading shows thermally stable, highly efficient, and tunable MA performance under different thicknesses and in the frequency range of 8.2–12.4 GHz and temperature range of 323–473 K. It could be seen that the samples with 3.2 mm possess the best MA performance. Meanwhile, double-belt absorption can be seen in the investigated range; it is superior to common single-belt absorption.[4,19,42] The maximum absorption in the two belts can be tuned from ~−10 to ~−15 dB and from ~−16 to ~−25 dB by varying temperature, respectively. With the increase of temperature, the intensity in the belt around −14 dB becomes stronger, while the intensity in the belt around −20 dB remains high. The belt for reflection loss (RL) ≤ −20 dB can almost cover the X band at 323 K.

The tunable feature of microwave absorption is attributed to the changeable impedance matching conditions and microwave attenuation in the interior absorber adjusted by varying the temperature.[62,63] Elevated temperature could decrease or increase the dielectric loss for the composites with different loading concentrations and slightly decrease the magnetic loss through the weakening effects to magnetism. A proper impedance matching condition would result in excellent MA properties. The microwave attenuation in the composites with 10 wt % loading, determined by attenuation constant α, is good and proper (Figure S8). The ability of varying temperature to tune absorption intensity indicates that the grape-like prototype can be a smart absorber.

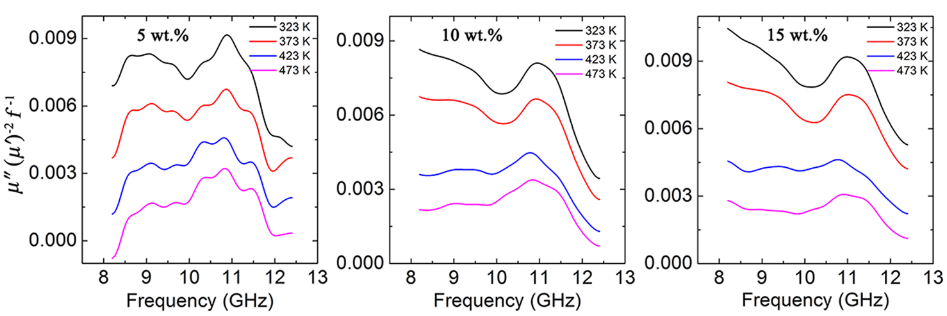

Figure 7. Frequency dependence of the $\mu''(\mu')^{-2}f^{-1}$ of grape-like Fe_3O_4-MWCNTs samples.

DOI: 10.1021/acsami.5b05595
ACS Appl. Mater. Interfaces 2015, 7, 19408–19415

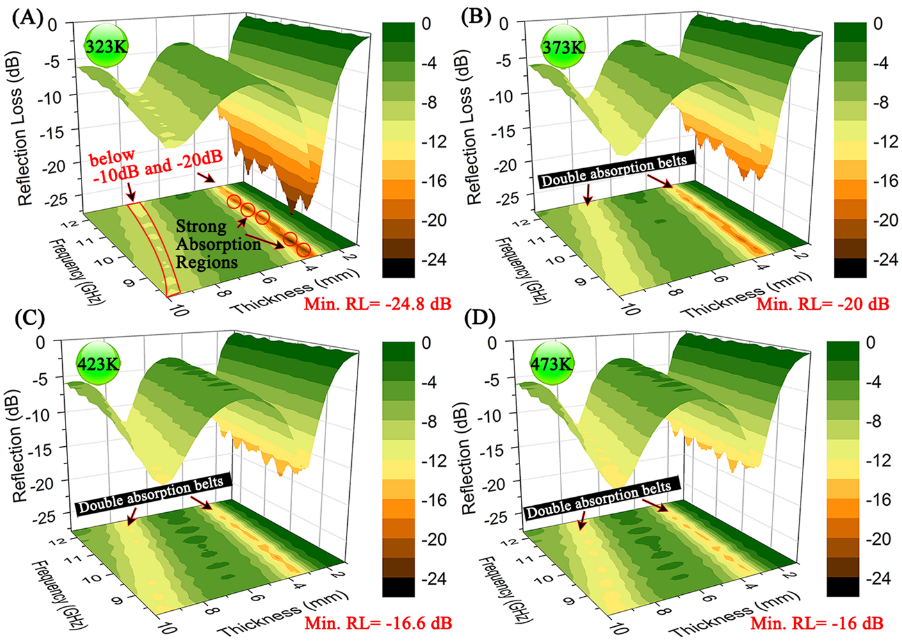

Figure 8. (A–D) Microwave absorption properties of the samples loaded with 10 wt % grape-like Fe_3O_4-MWCNTs versus the frequency and thickness at different temperatures.

■ CONCLUSIONS

In conclusion, multiscale-assembled grape-like Fe_3O_4-MWCNTs were fabricated through the coprecipitation method. The nanostructure demonstrates strong microwave absoprtion with tunable double-belt absorption in the temperature range of 323–473 K and X band. The maximum absorption in the two absorbing belts can be simultaneously tuned from ~−10 to ~−15 dB and from ~−16 to ~−25 dB by varying temperature, respectively. The tunable absorption is attributed to the impedance matching, benefiting from abundant interfacial polarizations and increased magnetic loss resulting from the grape-like Fe_3O_4 nanocrystals. Our findings provide a pathway to realize promising lightweight, high efficiency, and smart absorbers at elevated temperature.

■ EXPERIMENTAL SECTION

Materials. MWCNTs of 5–15 μm in length and 20–40 nm in diameter were obtained from Shenzhen Nanotech Port Co., Ltd. (China). HNO_3 solution (65–68 wt %), ferrous ammonium sulfate ($(NH_4)_2Fe(SO_4)_2{\cdot}6H_2O$), tetrahydrofuran (THF), ammonia–water, and deionized water were obtained from the Beijing Chemical Factory; ferric ammonium sulfate ($NH_4Fe(SO_4)_2{\cdot}12H_2O$) was obtained from Tianjin Fuchen Chemical Reagents Factory. High-purity SiO_2 xerogel nanopowders (99.9999 wt %) were purchased from North Star Special Ceramics Co., Ltd.. All of the reagents were used without further purication.

Modification of MWCNTs. One gram of MWCNTs was refluxed at 140 °C for 24 h in the mixture including 80 mL of nitric acid and 420 mL of deionized water. After refluxing, the precipitate was washed several times with deionized water until the pH ≈ 7. A dispersed suspension of MWCNTs can be obtained by treating the neutral aqueous solution of the precipitate by an ultrasonic cell disruptor for 1 h.

Multiscale-Assembled Fe_3O_4-MWCNTs Structure. The previous method reported was improved.[64] Typically, 20 mL of the suspension of MWCNTs (containing 100 mg of MWCNTs) was dispersed in 20 mL of aqueous solution containing 0.793 g of $NH_4Fe(SO_4)_2{\cdot}12H_2O$ and 0.322 g of $(NH_4)_2Fe(SO_4)_2{\cdot}6H_2O$. The mixture suspension was sonicated for 10 min; then, $NH_3{\cdot}H_2O$ (5 mL, 25 wt %) was dropwise added. After that, it was vigorously stirred for coprecipitating reaction at 50 °C for 5, 15, and 30 min. The resultant was centrifuged, and the precipitations were collected and washed thoroughly with deionized water and ethanol.

Samples. In a typical experiment, the Fe_3O_4-MWCNTs (5, 10, and 15 wt %) and SiO_2 xerogel nanopowder (95, 90, and 85 wt %) were added into the THF solvent with vigorous stirring to evaporate the solvent completely. A certain amount of the prepared mixture was pressed into a rectangular shape (22.86 mm × 10.16 mm) for electromagnetism parameter measurement. The test samples were adjusted with almost the same thickness of ~1.5 mm. The SiO_2-matrix MWCNTs samples were fabricated using the same method.

Measurement. XRD measurements were performed on an X′Pert PRO system (Cu Kα). Raman spectra were obtained on a HORIBA Jobin Yvon HR800 Raman spectrometer. Magnetic properties were measured by a Lakeshore 7407 vibrating sample magnetometer (VSM). SEM images were performed on a Hitachi S-4800 SEM system. TEM images were performed on a JEM-2100 TEM system, coupled with carbon or holey carbon coated copper grids. The high temperature DC conductivity was measured by a Keithley 2601A System SourceMeter coupled with sample heating equipment. The complex permittivity and permeability were measured on an Anritsu 37269D vector network analyzer by the waveguide method in the X band (8.2–12.4 GHz).

■ ASSOCIATED CONTENT

Ⓢ Supporting Information

The Supporting Information is available free of charge on the ACS Publications website at DOI: 10.1021/acsami.5b05595.

SEM images of the Sample I, Sample II, and Sample III; the particle size distribution of grape-like Fe_3O_4 nanocrystals; temperature dependences of the complex permittivity and permeability; frequency and temperature dependences of the tan δ_e and tan δ_m; the imaginary permittivity contributed by conductivity of the composites with 5, 10, and 15 wt % grape-like Fe_3O_4-MWCNTs loading; reflection loss of the samples with 5, 10, and 15 wt % loading concentration (PDF)

AUTHOR INFORMATION

Corresponding Authors

*E-mail: caomaosheng@bit.edu.cn.

*E-mail: yuanjie4000@sina.com.

Notes

The authors declare no competing financial interest.

ACKNOWLEDGMENTS

This research was supported by the National Science Foundation of China (Grant Nos. 51132002, 51372282, and 51072024).

REFERENCES

(1) Xia, T.; Zhang, C.; Oyler, N. A.; Chen, X. Hydrogenated TiO_2 Nanocrystals: A Novel Microwave Absorbing Material. *Adv. Mater.* **2013**, *25*, 6905−6910.

(2) Sun, H.; Chen, R. C.; You, X.; Jiang, Y. S.; Yang, Z. B.; Deng, J.; Qiu, L. B.; Peng, H. S. Cross-Stacking Aligned Carbon-Nanotube Films to Tune Microwave Absorption Frequencies and Increase Absorption Intensities. *Adv. Mater.* **2014**, *26*, 8120−8125.

(3) Dang, Z. M.; Zhou, T.; Yao, S. H.; Yuan, J. K.; Zha, J. W.; Song, H. T.; Li, J. Y.; Chen, Q.; Yang, W. T.; Bai, J. Advanced Calcium Copper Titanate/Polyimide Functional Hybrid Films with High Dielectric Permittivity. *Adv. Mater.* **2009**, *21*, 2077−2082.

(4) Wang, G. Z.; Gao, Z.; Tang, S. W.; Chen, C. Q.; Duan, F. F.; Zhao, S. C.; Lin, S. W.; Feng, Y. H.; Zhou, L.; Qin, Y. Microwave Absorption Properties of Carbon Nanocoils Coated with Highly Controlled Magnetic Materials by Atomic Layer Deposition. *ACS Nano* **2012**, *6*, 11009−11017.

(5) Yang, Y. L.; Gupta, M. C.; Dudley, K. L.; Lawrence, R. W. Conductive carbon nanoriber-polymer foam structures. *Adv. Mater.* **2005**, *17*, 1999−2003.

(6) Yang, H. J.; Cao, M. S.; Li, Y.; Shi, H. L.; Hou, Z. L.; Fang, X. Y.; Jin, H. B.; Wang, W. Z.; Yuan, J. Enhanced Dielectric Properties and Excellent Microwave Absorption of SiC Powders Driven with NiO Nanorings. *Adv. Opt. Mater.* **2014**, *2*, 214−219.

(7) Toneguzzo, P.; Viau, G.; Acher, O.; Fiévet-Vincent, F.; Fiévet, F. Monodisperse Ferromagnetic Particles for Microwave Applications. *Adv. Mater.* **1998**, *10*, 1032−1035.

(8) Zhao, D. L.; Li, X.; Shen, Z. M. Microwave absorbing property and complex permittivity and permeability of epoxy composites containing Ni-coated and Ag filled carbon nanotubes. *Compos. Sci. Technol.* **2008**, *68*, 2902−2908.

(9) Wang, J. C.; Xiang, C. S.; Liu, Q.; Pan, Y. B.; Guo, J. K. Ordered Mesoporous Carbon/Fused Silica Composites. *Adv. Funct. Mater.* **2008**, *18*, 2995−3002.

(10) Ding, L.; Tselev, A.; Wang, J. Y.; Yuan, D. N.; Chu, H. B.; McNicholas, T. P.; Li, Y.; Liu, J. Selective Growth of Well-Aligned Semiconducting Single-Walled Carbon Nanotubes. *Nano Lett.* **2009**, *9*, 800−805.

(11) Yang, Z. H.; Cao, Z.; Sun, H.; Li, Y. Composite Films Based on Aligned Carbon Nanotube Arrays and A Poly(N-isopropyl acrylamide) Hydrogel. *Adv. Mater.* **2008**, *20*, 2201−2205.

(12) Zheng, L. X.; O'Connell, M.; Doorn, S. K.; Liao, X. Z.; Zhao, Y. H.; Akhadov, E. A.; Hoffbauer, M. A.; Roop, B. J.; Jia, Q. X.; Dye, R. C.; Peterson, D. E.; Huang, S. M.; Liu, J.; Zhu, Y. T. Ultralong Single-Wall Carbon Nanotubes. *Nat. Mater.* **2004**, *3*, 673−676.

(13) Wang, F.; Dukovic, G.; Brus, L. E.; Heinz, T. F. The Optical Resonances in Carbon Nanotubes Arise from Excitions. *Science* **2005**, *308*, 838−841.

(14) Liu, X. M.; Yin, X. W.; Kong, L.; Li, Q.; Liu, Y.; Duan, W. Y.; Zhang, L. T.; Cheng, L. F. Fabrication and Electromagnetic Interference Shielding Effectiveness of Carbon Nanotube Reinforced Carbon Fiber/Pyrolytic Carbon Composites. *Carbon* **2014**, *68*, 501−510.

(15) Watts, P. C. P.; Hsu, W. K.; Barnes, A.; Chambers, B. High Permittivity from Defective Multiwalled Carbon Nanotubes in the X-band. *Adv. Mater.* **2003**, *15*, 600−603.

(16) Li, N.; Huang, Y.; Du, F.; He, X. B.; Lin, X.; Gao, H. J.; Ma, Y. F.; Li, F. F.; Chen, Y. S.; Eklund, P. C. Electromagnetic Interference (EMI) Shielding of Single-Walled Carbon Nanotube Epoxy Composites. *Nano Lett.* **2006**, *6*, 1141−1145.

(17) Yang, Y. L.; Gupta, M. C.; et al. Novel Carbon Nanotube-Polystyrene Foam Composites For Electromagnetic Interference Shielding. *Nano Lett.* **2005**, *5*, 2131−2134.

(18) Mahmoodi, M.; Arjmand, M.; Sundararaj, U.; Park, S. The Electrical Conductivity and Electromagnetic Interference Shielding of Injection Molded Multi-Walled Carbon Nanotube/Polystyrene Composites. *Carbon* **2012**, *50*, 1455−1464.

(19) Wen, B.; Cao, M. S.; Lu, M. M.; Shi, H. L.; Liu, J.; Wang, X. X.; Jin, H. B.; Fang, X. Y.; Wang, W. Z.; Yuan, J. Reduced Graphene Oxides: Light-Weight and High-Efficiency Electromagnetic Interference Shielding at Elevated Temperatures. *Adv. Mater.* **2014**, *26*, 3484−3489.

(20) Chen, Z. G.; Shi, Z. W.; Yang, W.; Lu, X. B.; Lai, Y.; Yan, H. G.; Wang, F.; Zhang, G. Y.; Li, Z. Q. Observation of An Intrinsic Bandgap and Landau Level Renormalization in Graphene/Boron-Nitride Heterostructures. *Nat. Commun.* **2014**, *5*, 4461.

(21) Yousefi, N.; Sun, X. Y.; Lin, X. Y.; Shen, X.; Jia, J. J.; Zhang, B.; Tang, B. Z.; Chan, M. S.; Kim, J. K. Highly Aligned Graphene/Polymer Nanocomposites with Excellent Dielectric Properties for High-Performance Electromagnetic Interference Shielding. *Adv. Mater.* **2014**, *26*, 5480−5487.

(22) Chen, Z. P.; Xu, C.; Ma, C. Q.; Ren, W. C.; Cheng, H. M. Lightweight and Flexible Graphene Foam Composites for High-Performance Electromagnetic Interference Shielding. *Adv. Mater.* **2013**, *25*, 1296−1300.

(23) Wen, B.; Wang, X. X.; Cao, W. Q.; Shi, H. L.; Lu, M. M.; Wang, G.; Jin, H. B.; Wang, W. Z.; Yuan, J.; Cao, M. S. Reduced Graphene Oxides: the Thinnest and Most Lightweight Materials with Highly Efficient Microwave Attenuation Performances of the Carbon World. *Nanoscale* **2014**, *6*, 5754−5761.

(24) Yan, D. X.; Pang, H.; Li, B.; Vajtai, R.; Xu, L.; Ren, P. G.; Wang, J. H.; Li, Z. M. Structured Reduced Graphene Oxide/Polymer Composites for Ultra-Efficient Electromagnetic Interference Shielding. *Adv. Funct. Mater.* **2015**, *25*, 559−566.

(25) Zhang, Y.; Huang, Y.; Zhang, T. F.; Chang, H. C.; Xiao, P. S.; Chen, H. H.; Huang, Z. Y.; Chen, Y. S. Broadband and Tunable High-Performance Microwave Absorption of an Ultralight and Highly Compressible Graphene Foam. *Adv. Mater.* **2015**, *27*, 2049−2053.

(26) Liu, W. W.; Li, H.; Zeng, Q. P.; Duan, H. N.; Guo, Y. P.; Liu, X. F.; Sun, C. Y.; Liu, H. Z. Fabrication of Ultralight Three-Dimensional Graphene Networks with Strong Electromagnetic Wave Absorption Properties. *J. Mater. Chem. A* **2015**, 3, 3739−3747.

(27) Han, M. K.; Yin, X. W.; Kong, L.; Li, M.; Duan, W. Y.; Zhang, L. T.; Cheng, L. F. Graphene-Wrapped ZnO Hollow Spheres with Enhanced Electromagnetic Wave Absorption Properties. *J. Mater. Chem. A* **2014**, *2*, 16403−16409.

(28) Wu, F.; Xia, Y. L.; Wang, Y.; Wang, M. Y. Two-step Reduction of Self-Assembed Three-Dimensional (3D) Reduced Graphene Oxide (RGO)/Zinc Oxide (ZnO) Nanocomposites for Electromagnetic Absorption. *J. Mater. Chem. A* **2014**, *2*, 20307−20315.

(29) Sun, X. M.; Zhang, Z. T.; Lu, X.; Guan, G. Z.; Li, H. P.; Peng, H. S. Electric Current Test Paper Based on Conjugated Polymers and Aligned Carbon Nanotubes. *Angew. Chem., Int. Ed.* **2013**, *52*, 7776−7780.

(30) Gupta, T. K.; Singh, B. P.; Mathur, R. B.; Dhakate, S. R. Multi-Walled Carbon Nanotube-Graphene-Polyaniline Multiphase Nanocomposite with Superior Electromagnetic Shielding Effectiveness. *Nanoscale* **2014**, *6*, 842−851.

(31) Zhang, H. L.; Li, J. F.; Zhang, B. P.; Yao, K. F.; Liu, W. S.; Wang, H. Electrical and Thermal Properties of Carbon Nanotube Bulk Materials: Experimental Studies for the 328−958 K Temperature Range. *Phys. Rev. B: Condens. Matter Mater. Phys.* **2007**, *75*, 205407.

DOI: 10.1021/acsami.5b05595
ACS Appl. Mater. Interfaces 2015, 7, 19408−19415

(32) Wang, Y.; Di, C. A.; Liu, Y. Q.; Kajiura, H.; Ye, S. H.; Cao, L. C.; Wei, D. C.; Zhang, H. L.; Li, Y. M.; Noda, K. Optimizing Single-Walled Carbon Nanotube Films for Applications in Electroluminescent Devices. *Adv. Mater.* **2008**, *20*, 4442−4449.

(33) Wen, J. F.; Zhang, Y.; Tang, N. J.; Wan, X. G.; Xiong, Z. H.; Zhong, W.; Wang, Z. L.; Wu, X. L.; Du, Y. W. Synthesis, Photoluminescence, and Magnetic Properties of Nitrogen-Doping Helical Carbon Nanotubes. *J. Phys. Chem. C* **2011**, *115*, 12329−12334.

(34) Dang, Z. M.; Yao, S. H.; Yuan, J. K.; Bai, J. B. Tailored Dielectric Properties based on Microstructure Change in BaTiO3-Carbon Nanotube/Polyvinylidene Fluoride Three-Phase Nanocomposites. *J. Phys. Chem. C* **2010**, *114*, 13204−13209.

(35) Kong, L.; Yin, X. W.; Yuan, X. Y.; Zhang, Y. J.; Liu, X. M.; Cheng, L. F.; Zhang, L. T. Electromagnetic Wave Absorption Properties of Graphene Modified with Carbon Nanotube/Poly-(dimethyl siloxane) Composites. *Carbon* **2014**, *73*, 185−193.

(36) Che, R. C.; Peng, L. M.; Duan, X. F.; Chen, Q.; Liang, X. L. Microwave Absorption Enhancement and Complex Permittivity and Permeability of Fe Encapsulated within Carbon Nanotubes. *Adv. Mater.* **2004**, *16*, 401−405.

(37) Wang, Z. J.; Wu, L. N.; Zhou, J. G.; Jiang, Z. H.; Shen, B. Z. Chemoselectivity-Induced Multiple Interfaces in MWCNT/Fe_3O_4@ZnO Heterotrimers for Whole X-band Microwave Absorption. *Nanoscale* **2014**, *6*, 12298−12302.

(38) Wang, Z. J.; Wu, L. N.; Zhou, J. G.; Cai, W.; Shen, B. Z.; Jiang, Z. H. Magnetite Nanocrystals on Multiwalled Carbon Nanotubes as a Synergistic Microwave Absorber. *J. Phys. Chem. C* **2013**, *117*, 5446−5452.

(39) Wen, F. S.; Zhang, F.; Liu, Z. Y. Investigation on Microwave Absorption Properties for Multiwalled Carbon Nanotubes/Fe/Co/Ni Nanopowders as Lightweight Absorbers. *J. Phys. Chem. C* **2011**, *115*, 14025−14030.

(40) Liu, J.; Cheng, J.; Che, R.; Xu, J.; Liu, M.; Liu, Z. Synthesis and Microwave Absorption Properties of Yolk−Shell Microspheres with Magnetic Iron Oxide Cores and Hierarchical Copper Silicate Shells. *ACS Appl. Mater. Interfaces* **2013**, *5*, 2503−2509.

(41) Tong, G. X.; Liu, F. T.; Wu, W. H.; Du, F. F.; Guan, J. G. Rambutan-Like Ni/MWCNT Heterostructures: Easy Synthesis, Formation Mechanism, and Controlled Static Magnetic and Microwave Electromagnetic Characteristics. *J. Mater. Chem. A* **2014**, *2*, 7373−7382.

(42) Wang, G. Z.; Gao, Z.; Wan, G. P.; Lin, S. W.; Yang, P.; Qin, Y. High Densities of Magnetic Nanoparticles Supported on Graphene Fabricated by Atomic Layer Deposition and Their Use as Efficient Synergistic Microwave Absorbers. *Nano Res.* **2014**, *7*, 704−716.

(43) Ren, Y. L.; Wu, H. Y.; Lu, M. M.; Chen, Y. J.; Zhu, C. L.; Gao, P.; Cao, M. S.; Li, C. Y.; Ouyang, Q. Y. Quaternary Nanocomposites Consisting of Graphene, Fe3O4@Fe Core@Shell, and ZnO Nanoparticles: Synthesis and Excellent Electromagnetic Absorption Properties. *ACS Appl. Mater. Interfaces* **2012**, *4*, 6436−6442.

(44) Yang, Z.; Li, Z.; Yang, Y.; Xu, Z. J. Optimization of ZnxFe3-xO4 Hollow Spheres for Enhanced Microwave Attenuation. *ACS Appl. Mater. Interfaces* **2014**, *6*, 21911−21915.

(45) Pan, G.; Zhu, J.; Ma, S.; Sun, G.; Yang, X. Enhancing the Electromagnetic Performance of Co through the Phase-Controlled Synthesis of Hexagonal and Cubic Co Nanocrystals Grown on Graphene. *ACS Appl. Mater. Interfaces* **2013**, *5*, 12716−12724.

(46) Liang, C. Y.; Liu, C. Y.; Wang, H.; Wu, L. N.; Jiang, Z. H.; Xu, Y. J.; Shen, B. Z.; Wang, Z. J. SiC-Fe_3O_4 Dielectric-Magnetic Hybrid Nanowires: Controllable Fabrication, Characterization and Electromagnetic Wave Absorption. *J. Mater. Chem. A* **2014**, *2*, 16397−16402.

(47) Wang, H.; Wu, L. N.; Jiao, J. G.; Xu, Y. J.; Zhang, H. Y.; Jiang, Z. H.; Shen, B. Z.; Wang, Z. J. Covalent Interaction Enhanced Electromagnetic Wave Absorption in SiC/Co Hybrid Nanowires. *J. Mater. Chem. A* **2015**, *3*, 6517−6525.

(48) Liu, C. Y.; Xu, Y. J.; Wu, L. N.; Jiang, Z. H.; Shen, B. Z.; Wang, Z. J. Fabrication of Core-Multishell MWCNT/Fe_3O_4/PANI/Au Hybrid Nanotubes with High-Performance Electromagnetic Absorption. *J. Mater. Chem. A* **2015**, *3*, 10566−10572.

(49) Wang, Z. J.; Wu, L. N.; Zhou, J. G.; Shen, B. Z.; Jiang, Z. H. Enhanced Microwave Absorption of Fe_3O_4 Nanocrystals after Heterogeneously Growing with ZnO Nanoshell. *RSC Adv.* **2013**, *3*, 3309−3315.

(50) Liu, J. W.; Che, R. C.; Chen, H. J.; Zhang, F.; Xia, F.; Wu, Q. S.; Wang, M. Microwave Absorption Enhancement of Multifunctional Composite Microspheres with Spinel Fe_3O_4 Cores and Anatase TiO_2 Shells. *Small* **2012**, *8*, 1214−1221.

(51) Sun, G. B.; Dong, B. X.; Cao, M. H.; Wei, B. Q.; Hu, C. W. Hierarchical Dendrite-Like Magnetic Materials of Fe_3O_4, gamma-Fe_2O_3, and Fe with High Performance of Microwave Absorption. *Chem. Mater.* **2011**, *23*, 1587−1593.

(52) Du, Y. C.; Liu, W. W.; Qiang, R.; Wang, Y.; Han, X. J.; Ma, J.; Xu, P. Shell Thickness-Dependent Microwave Absorption of Core-Shell Fe_3O_4@C Composites. *ACS Appl. Mater. Interfaces* **2014**, *6*, 12997−13006.

(53) Yang, H. J.; Cao, W. Q.; Zhang, D. Q.; Su, T. J.; Shi, H. L.; Wang, W. Z.; Yuan, J.; Cao, M. S. NiO Hierarchical Nanorings on SiC: Enhancing Relaxation to Tune Microwave Absorption at Elevated Temperature. *ACS Appl. Mater. Interfaces* **2015**, *7*, 7073−7077.

(54) Zhang, T.; Zhong, B.; Yang, J. Q.; Huang, X. X.; Wen, G. Boron and Nitrogen Doped Carbon Nanotubes/Fe_3O_4 Composite Architectures with Microwave Absorption Property. *Ceram. Int.* **2015**, *41*, 8163−8170.

(55) Qiu, J.; Qiu, T. T. Fabrication and Microwave Absorption Properties of Magnetite Nanoparticle-Carbon Nanotube-Hollow Carbon Fiber Composites. *Carbon* **2015**, *81*, 20−28.

(56) Chen, Y. H.; Huang, Z. H.; Lu, M. M.; Cao, W. Q.; Yuan, J.; Zhang, D. Q.; Cao, M. S. 3D Fe_3O_4 Nanocrystals Decorating Carbon Nanotubes to Tune Electromagnetic Properties and Enhance Microwave Absorption Capacity. *J. Mater. Chem. A* **2015**, *3*, 12621−12625.

(57) Guo, L.; Liang, F.; Wen, X. G.; Yang, S. H.; He, L.; Zheng, W. Z.; Chen, C. P.; Zhong, Q. P. Uniform Magnetic Chains of Hollow Cobalt Mesospheres from One-Pot Synthesis and Their Assembly in Solution. *Adv. Funct. Mater.* **2007**, *17*, 425−430.

(58) Park, J.; An, K. J.; Hwang, Y. S.; Park, J. G.; Noh, H. J.; Kim, J. Y.; Park, J. H.; Hwang, N. M.; Hyeon, T. Ultra-Large-Scale Syntheses of Monodisperse Nanocrystals. *Nat. Mater.* **2004**, *3*, 891−895.

(59) Liu, J.; Cao, W. Q.; Jin, H. B.; Yuan, J.; Zhang, D. Q.; Cao, M. S. Enhanced Permittivity and Multi-Region Microwave Absorption of Nanoneedle-Like ZnO in X-band at Elevated Temperature. *J. Mater. Chem. C* **2015**, *3*, 4670−4677.

(60) Aharoni, A. Effect of Surface Anisotropy on the Exchange Resonance Modes. *J. Appl. Phys.* **1997**, *81*, 830−833.

(61) Arias, R.; Chu, P.; Mills, D. L. Dipole Exchange Spin Waves and Microwave Response of Ferromagnetic Spheres. *Phys. Rev. B: Condens. Matter Mater. Phys.* **2005**, *71*, 224410.

(62) Qin, F.; Brosseau, C. A Review and Analysis of Microwave Absorption in Polymer Composites Filled with Carbonaceous Particles. *J. Appl. Phys.* **2012**, *111*, 061301.

(63) Yan, S. J.; Zhen, L.; Xu, C. Y.; Jiang, J. T.; Shao, W. Z. Microwave Absorption Properties of $FeNi_3$ Submicrometre Spheres and SiO_2@$FeNi_3$ Core-Shell Structures. *J. Phys. D: Appl. Phys.* **2010**, *43*, 245003.

(64) Liu, Z.; Wang, J.; Xie, D. H.; Chen, G. Polyaniline-Coated Fe_3O_4 Nanoparticle-Carbon-Nanotube Composite and its Application in Electrochemical Biosensing. *Small* **2008**, *4*, 462−466.

DOI: 10.1021/acsami.5b05595
ACS Appl. Mater. Interfaces 2015, 7, 19408−19415